Korean J. Chem. Eng., 34(4), 1199-1207 (2017)
DOI: 10.1007/s11814-017-0014-4

pISSN: 0256-1115
eISSN: 1975-7220

Photocatalytic degradation of methylene blue in aqueous solution using ceramsite coated with micro-Cu_2O under visible-light irradiation

Tianpeng Li*, Tingting Sun, Tallal Bin Aftab*, and Dengxin Li*,†**

*College of Environment Science and Engineering, Donghua University, Shanghai 201620, China
**School of Basic Medical Science, Wenzhou Medical University, Wenzhou 325035, Zhejiang Province, China
(*Received 19 August 2016 • accepted 2 February 2017*)

Abstract−A novel ceramsite coated with micro-cuprous oxide (Cu_2O) catalyst was prepared and its photocatalytic activity was investigated by determining the degradation of methylene blue (MB) in aqueous solutions under Xe light. The results showed that the catalyst had many outstanding characteristics, such as higher BET specific surface area, larger pore size and stronger visible-light adsorption capacity, suggesting that it is a promising photocatalytic material. Under experimental conditions the initial concentration was 15 mg/L, pH was 3 and photocatalyst dosage was 0.5 g, and the degradation rate of MB reached 93.31% after Xe light was irradiated for 75 min. The photocatalytic degradation of MB followed the pseudo-first-order kinetics model, with high correlation coefficient values (R^2>0.95). Some major degradation intermediates and desired products were identified by GC-MS and IC, respectively. Finally, the degradation pathways of MB by the catalyst under Xe light were proposed.

Keywords: Ceramsite, Micro-Cu_2O, Photocatalytic Activity, Visible-light Adsorption, Degradation Pathway

INTRODUCTION

Photocatalysis has been extensively studied for the treatment of contaminated water [1-4]. The technology belongs to advanced oxidation process (AOP), which can decompose pollutants in the presence of nano/micro-meter semiconductor catalyst and ultraviolet or visible-light illumination, without adding any oxidation agents. Among various nano/micro-meter semiconductors [5-7], nano/micro-Cu_2O is one of the first known p-type semiconductors with a narrow direct band gap of 2.0-2.2 eV [8,9]. Micro-Cu_2O has been considered as a potential practical candidate in environmental pollution control, because it is found naturally in abundance, low-cost production processing, nontoxic nature, decomposition of water into O_2 and H_2 molecules, degradation of organic pollutants and sensing gas under visible-light irradiation (λ<620 nm) [10-13]. Many researchers have suggested that nano/micro-particles are difficult to recycle and reuse, especially in the field of wastewater treatment, because they are too small and tend to aggregate [14]. On the other hand, the stability of nano/micro-particles is a serious issue in oxidation-reduction reactions [15]. The problems have hindered the implementation of the particles in the full-scale treatment of sewage. Previously, reports have demonstrated that nano/micro-particle coating is an available method to resolve the above problems [16,17].

Ceramsite, with high total porosity, large specific surface area, low bulk and apparent density, has been widely used as building material [18], as well as filter media in wastewater treatment [19]. Commonly, raw materials used for production of ceramsite are mainly dependent on non-renewable natural resources, such as clay [20] and shale [21], which may threaten sustainable development of nature in the long run. For the protection of natural resources, it is very significant to find an appropriate substitute for natural resources. Fortunately, due to similar mineral content, more and more municipal solid wastes have been selected as a potential substitute to replace natural resources for production of ceramsite [22,23]. Ceramsite exhibits many prominent properties, such as chemical stability and mechanical properties, versatility of structural properties, and it has functional groups on the surface [24-26]. With the increase in demand for multi-functional composite ceramsite materials, they are being fabricated through coupling technique, surface modification technology or coating method, such as bio-ceramsite was fabricated by *Citrobacter freundii* (*C. freundii*) immobilization on the ceramsite [27], porous ceramsite was modified using a magnetic material (pure Fe_3O_4) [28], ceramic microfilters coated with colloidal zirconia [29], nano-TiO_2 thin film coated on porous ceramic filter media (PCFM) by sol-gel process [30] and a new nanocomposite for water disinfection was prepared by self-aggregation of silver nanoparticles on the surface of ceramsite [31].

Referencing the above discussion, the present study was conducted as follows. First, micro-Cu_2O was prepared by a liquid-phase reduction method; simultaneously, ceramsite coated with micro-Cu_2O catalyst was prepared via dipcoating method. Second, the catalyst was characterized by XRD, SEM, BET and UV-vis. Third, the photocatalytic activity of the catalyst was assessed by the degradation of MB in aqueous solution under visible-light irradiation, and then the photocatalytic degradation kinetics was analyzed. Finally, the degradation products were identified by GC-MS and IC, and then the degradation pathway of MB during the photocat-

†To whom correspondence should be addressed.
E-mail: lidengxin@dhu.edu.cn

alytic degradation process was proposed.

EXPERIMENTAL

1. Materials and Chemicals

The dewatered sewage sludge (DSS), coal fly ash (CFA) and river sediment were obtained from Shanghai Songjiang Sewage Treatment Plant, Shanghai Waigaoqiao Power Generation Co. Ltd. and Songjiang Campus of Donghua University, China, respectively. Analytical grade of copper (II) sulfate pentahydrate ($CuSO_4 \cdot 5H_2O$), hydrazine hydrate ($N_2H_4 \cdot H_2O$), sodium hydroxide (NaOH), dodecyl trimethyl ammonium bromide (DTAB), perchloric acid ($HClO_4$) and MB were purchased from Sinopharm Chemical Reagent Co., Ltd., China. All chemicals were used as received without further purification. Deionized water was used in all experiments.

2. Preparation

2-1. Ceramsite

The ceramsite (about 10-mm-diameter) used in this study was obtained from DSS, CFA and river sediment, without using any natural resources, and it was prepared by a high-temperature sintering process. The results of the composition of DSS, CFA and river sediment, the preparation procedure, the temperature control of high-temperature sintering, the physical properties and heavy metal leaching toxicity of ceramsite were presented in our previous researches [32,33]. To be specific, compared with natural resources, such as shale and clay, the composition of raw materials, such as SiO_2, Al_2O_3, Fe_2O_3, CaO, MgO, Na_2O and K_2O, was basically the same. The physical properties of ceramsite, such as breaking and wear rate (0.2%), solubility in hydrochloric acid (0.01%), silt carrying capacity (0.2%), void fraction (71.1%) and BET specific surface area (0.75×10^4 cm^2/g), met with the China's industrial standard of Artificial Ceramsite Filter Material for Water Treatment (CJ/T 299-2008). The lixiviation tests results demonstrated that only few heavy metals (such as Cr, Zn and Cu) were found in the lixivium, with the content much lower than the national threshold of Identification Standards for Hazardous Wastes-Identification for Extraction Toxicity (GB 5085.3-2007, China). In brief, the results demonstrate that the lab-made ceramsite is safe, reliable and can be further studied and applied as filter media, adsorbent or other media/materials in wastewater treatment.

Prior to the application, the as-prepared ceramsite was crushed down and sieved to a diameter of about 1 mm. Consequently, it was etched in $HClO_4$ (50%, V/V) for approximately 10 min under mechanical agitating, to remove any impurities, and then rinsed with water and dried at 80 °C for 180 min.

2-2. Ceramsite Coated with Micro-Cu_2O

The micro-Cu_2O was synthesized using $CuSO_4 \cdot 5H_2O$ and $N_2H_4 \cdot H_2O$ as copper source and reductant, respectively. The synthesis mechanism of micro-Cu_2O is described as follows:

$$CuSO_4 \cdot 5H_2O + 2NaOH = Cu(OH)_2 + Na_2SO_4 + 5H_2O \quad (1)$$

$$4Cu(OH)_2 + N2H_4 \cdot H_2O = 2Cu_2O + N_2 \uparrow + 7H_2O \quad (2)$$

Based on Eqs. (1) and (2), the optimal molar ratio of $CuSO_4 \cdot 5H_2O$, NaOH and $N_2H_4 \cdot H_2O$ was 1 : 2 : 0.25. In addition, the mass ratio of $CuSO_4 \cdot 5H_2O$ and ceramsite was selected 5 : 1. Briefly, ceramsite was dissolved in the mixture of 90 mL deionized water, $CuSO_4 \cdot 5H_2O$ and DTAB with electromagnetic stirring at 60 °C for 20 min. Subsequently, in total 8 g of NaOH was added to the mixture in small amounts in equal intervals. After stirring at 60 °C for 20 min, 10 mL $N_2H_4 \cdot H_2O$ solution (2.5 mol/L) was added by dripping slowly and stirring continued at 70 °C for 150 min. After this, the ceramsite was coated with micro-Cu_2O of which a Cu_2O content of about 10-15% (wt) was obtained after being centrifuged and dried in vacuum drying oven at 50 °C for over 10 h. The reaction mixture underwent a series of color changes from blue, dark green and finally to orange yellow.

3. Photocatalytic Activity

500 mg/L stock solution was prepared by dissolving an appropriate quantity of MB in deionized water. 50 mL volume simulated wastewater in different concentrations of MB in the range of 5-30 mg/L was prepared by stepwise dilution of the stock solution.

The ceramsite coated with micro-Cu_2O catalyst was irradiated under an adjustable-type Xe lamp (XQ350W, Shanhai blue Sheng Electronic Co., Ltd., China) at room temperature of 25±5 °C to study the photocatalytic activity. The schematic diagram for the degradation of MB was illustrated in Fig. 1. Typically, a 50 mL solution of MB was placed in glass beaker, after initial pH of the solution was adjusted with 0.1 M NaOH or 0.1 M HCl to obtain the designated value; 0.5 g ceramsite coated with micro-Cu_2O catalyst was added in this solution. Then, the glass beaker was magnetically stirred under the protection from light condition, to establish an adsorption/desorption equilibrium between MB molecules and the surface of the photocatalyst [34]. After absorption for 20 min, the glass beaker was illuminated by the Xe lamp (λ>420 nm). At given time intervals, the MB concentration in filtrate was monitored. All the degradation experiments were performed twice under the same conditions and an averaged value was used.

4. Analysis

Crystalline phases of samples were characterized by X-ray diffraction (XRD, D/max-2550 PC, Shimadzu Corporation, Japan) with CuK radiation (λ=0.1548 nm) at 40 kV and 40 mA. A scanning electron microscope (SEM, Quanta-250, Fei Instrument, Czech) was used to observe the surface morphology of samples with an accelerating voltage of 13 kV. Before measurement, the surface of sam-

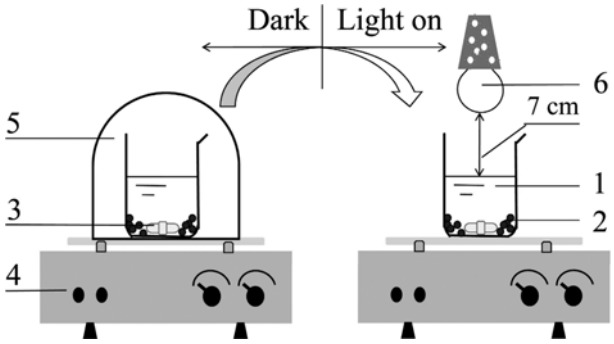

Fig. 1. Schematic diagram for the degradation of MB.

1. MB solution
2. Ceramsite coated with micro-Cu_2O catalyst
3. Stir bar
4. Magnetic stirrer
5. Cover
6. Xe lamp

ples was sputtered with gold layer to improve the quality of the images. The Brunauer-Emmett-Teller (BET) specific surface area, S_{BET}, was calculated from N_2 adsorption and desorption measurements obtained using fully automatic specific and micro pore size analyzer (AUTOSORB-IQ2-MP, USA). Pore size distribution over the mesopore range was generated by the Barrett-Joyner-Halenda (BJH) analysis of the desorption branches, and the values for the average pore size were calculated. The ultraviolet-visible transmission spectra of samples were determined with a spectrophotometer (UV-vis, UV-3600, PerkinElmer, USA). Degradation intermediates of MB were identified by gas chromatography-mass spectrometry (GC-MS) analyses. The GC-MS was performed on Shimadzu GC-MS QP 2010 instrument (DB-5 ms, 30 m×0.25 mm×0.25 μm) with column flow-1.0 mL/min, 40-280 °C at 10 °/min rise. According to the previous studies [35], the concentration of negative inorganic ions, such as sulfate (SO_4^{2-}) and nitrate (NO_3^-) in the filtrate, was determined by an ICS-90 ion chromatography system (IC, Dionex, USA) equipped with an Ionpac AG14 guard column and an Ionpac AS14 analytical column. The MB concentration was measured by UV-vis spectrophotometry (UV754N, INESA analytical instrument Co., Ltd., China) at its maximum wavelength (λ_{max}) of 664 nm. The degradation rate was calculated by the following equation:

$$D = \frac{C_0 - C_t}{C_0} \times 100\% \quad (3)$$

where D is the degradation rate of MB, %; C_0 and C_t are the concentrations of MB at '0'and 't' min, respectively, mg/L.

RESULTS AND DISCUSSION

1. Characterization

1-1. Crystalline Phases

Crystalline phase analyses of samples were elucidated by XRD, and the results listed in Fig. 2. As shown in Fig. 2(a), the chemical compositions of ceramsite were metal oxides and metal compounds, such as syn-Fe_2O_3, Quartz-SiO_2, Chromium Vanadium Oxide, Albite, Labradorite and Anorthite, that were mainly attributed to the raw materials composition. Compared with the crystalline phases of ceramsite, on the crystalline phases of ceramsite coated with micro-Cu_2O catalyst appeared five obvious characteristic peaks at 2θ values of 29.46°, 36.56°, 42.42°, 61.52° and 73.6° (Fig. 2(b)), which corresponds to the crystal planes of {110}, {111}, {200}, {220} and {311}, respectively [36]. The XRD pattern confirmed that the formation of micro-Cu_2O and the obtained results agree with the standard crystal of Cu_2O (JCPDS No. 05-0667). According to the previous studies [37], these characteristic peaks belong to the Cu-O vibration of Cu_2O crystals. Hence, the ceramsite coated with micro-Cu_2O catalyst has photocatalytic activity. This activity was determined by the characteristics of their crystal structure; for instance, the photocatalytic activity with different crystal planes followed the order {111}>{110} [38]. Thus, we can draw a conclusion that novel ceramsite coated with micro-Cu_2O catalyst can be obtained under the experimental conditions.

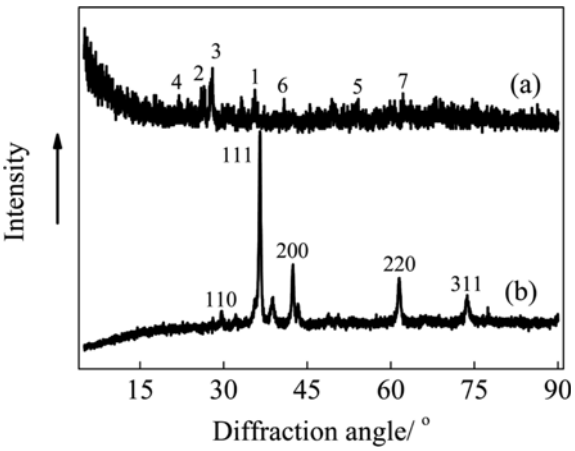

Fig. 2. XRD patterns of (a) ceramsite (1: Hematite, 2: Quartz-SiO_2, 3: Albite, Ca-rich; 4: Labradorite-$Ca_{0.64}Na_{0.35}(Al_{1.63}Si_{2.37}O_8)$; 5: Albite low-Na($AlSi_3O_8$); 6: Anorthite-Ca($Al_2Si_2O_8$); 7: Chromium vanadium oxide) and (b) ceramsite coated with micro-Cu_2O catalyst.

1-2. Surface Morphology

The surface morphology of samples was observed by SEM, and the results presented in Fig. 3. The rough surface and porous structure were extremely obvious (shown in Fig. 3(a) and (b)). There were many impurities dispersed on the surface and pores of the ceramsite before pretreatment (Fig. 3(a)). However, almost all the impurities disappeared after pretreatment, and the surface and pores of the ceramsite became quite smooth and highly polished (Fig. 3(b)). The main purpose of pretreatment is to increase pore size of ceramsite and gain additional active sites of ceramsite, contributing to coating with more micro-Cu_2O. Micro-Cu_2O was obtained with particle diameter of 200-400 nm, as displayed in Fig. 3(c). A high-resolution image of micro-Cu_2O is shown in Fig. 3(d); we found that the micro-Cu_2O shows elliptic and flat, which corresponds to the results obtained by low-magnification SEM result. The surface and pores of the ceramsite became rough again and the apparent delamination phenomenon appeared (depicted in Fig. 3(e) and (f)). It indicated that there were vast quantities of deposits on the surface and pores of the ceramsite. According to the results of Fig. 2, we firmly believe that the sediments were micro-Cu_2O. Micro-analysis illustrated that a multiplex porous structure, associated with a large amount of micro-Cu_2O, was developed on the surface and pores of ceramsite after the coating treatment (seen Fig. 3(f)). Fig. 3(e) and f show that micro-Cu_2O was deposited not only on the surface of ceramsite, but also on the pores of ceramsite, and the latter was superior to the former, because the latter did not easily fall off. Therefore, it is not difficult to sum up that micro-Cu_2O coating on ceramsite was just a physical combination and the chemical stability, reactive activity and treatment efficiency were confirmed by many factors.

1-3. Pore Size Distribution

Typical N_2 adsorption-desorption isotherms of samples were investigated, and the results presented in Fig. 4. The adsorption-desorption patterns of the two samples belong to the typical IUPAC IV-type with the H_2-type hysteresis loop, which characterizes mesoporous solids. The hysteresis loop, of H_2-type, can be explained as the distribution of pore sizes and pore shapes are not well defined

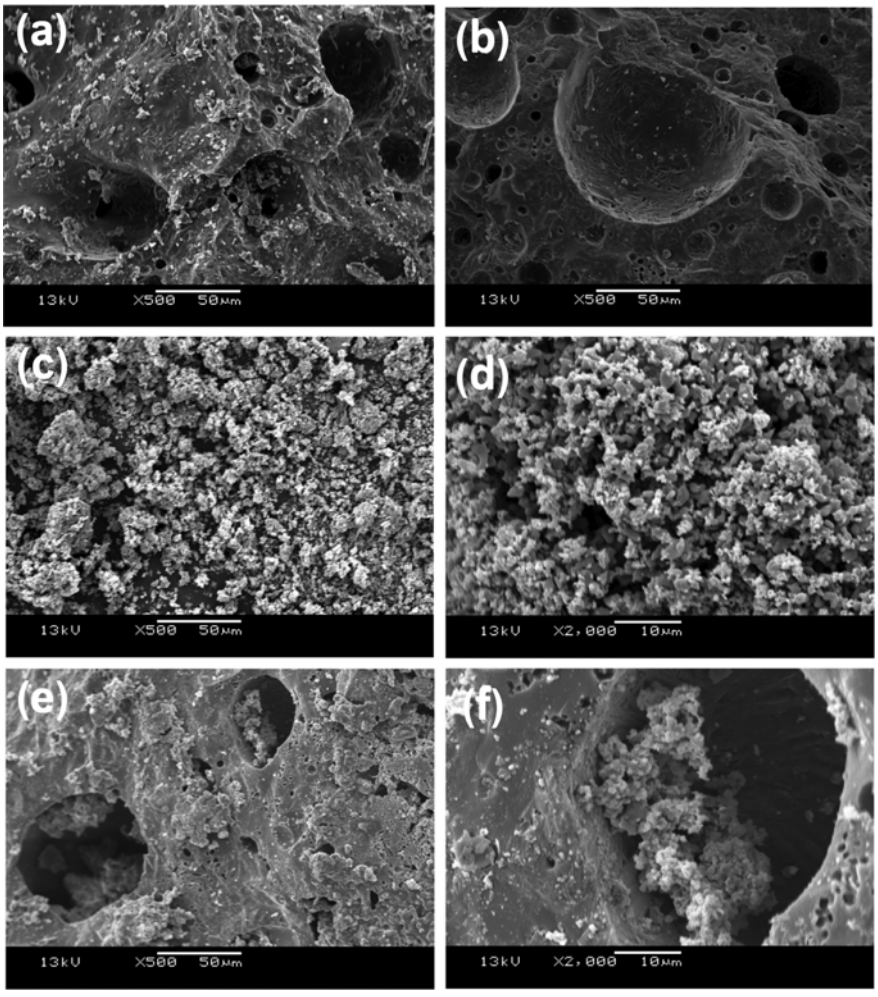

Fig. 3. SEM images of (a) before pretreatment of ceramsite, (b) pretreated ceramsite, (c), (d) as-prepared micro-Cu_2O and (e), (f) ceramsite coated with micro-Cu_2O catalyst.

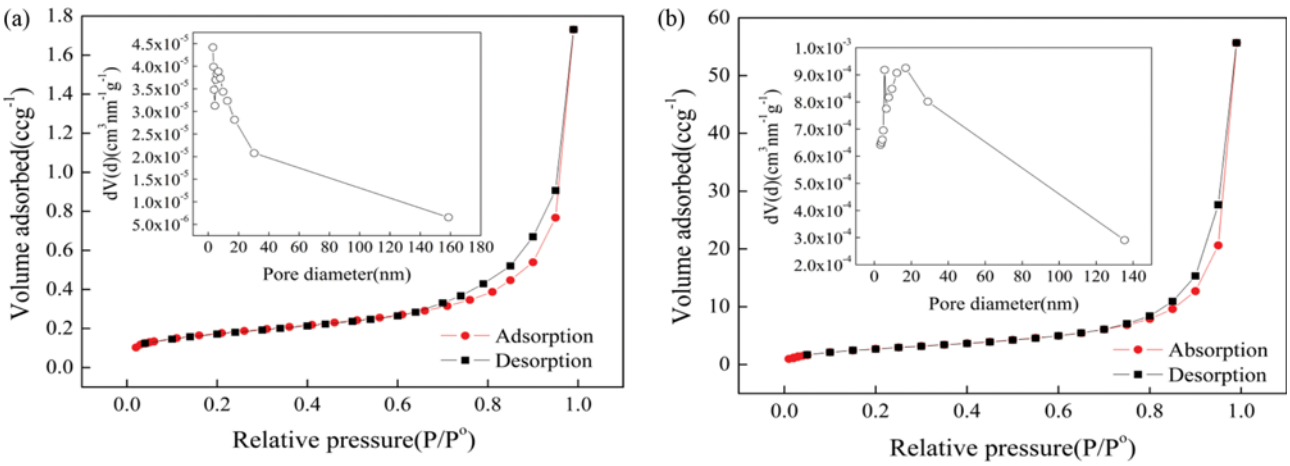

Fig. 4. N_2 adsorption-desorption isotherms and pore size distribution (inset) of samples.
(a) Ceramsite, (b) Nanocomposite ceramsite material

or are irregular [39], which is commonly attributed to slit-shaped pores generated by the aggregation of plate-like particles [40]. From Fig. 4, it is evident that both of the two samples show type IV isotherms with hysteresis loop at P/P_0=0.45 to 0.95, and the isotherms

Table 1. Textural properties of samples from N_2 adsorption-desorption isotherms

Samples	S_{BET} (m^2/g)	Pore volume (m^3/g)	Pore size (nm)
Ceramsite	0.63	0.003	16.97
Micro-Cu_2O	15.39	0.091	118.9
Ceramsite coated with micro-Cu_2O	10.37	0.086	166.1

show high absorption at high relative pressure P/P_0=0.99. Moreover, each sample exhibits a similar type of hysteresis loop, suggesting that pore size and shape are basically the same in these samples. The pore size distribution patterns of the samples are shown in the inset of Fig. 4. Ceramsite coated with micro-Cu_2O catalyst shows a narrower pore size distribution than that of ceramsite. This is probably because the micro-Cu_2O was deposited on the pores of ceramsite, reducing its pore size (seen Fig. 3(e) and (f)).

The textural properties of samples from N_2 adsorption-desorption isotherms are tabulated in Table 1. The S_{BET}, pore volume and size of micro-Cu_2O are 24.43, 30.33 and 7.01-times more than that of ceramsite only, respectively. Additionally, after being coated with micro-Cu_2O, the S_{BET}, pore volume and size of ceramsite increased by 93.92%, 96.51% and 89.78%, respectively. The results demonstrate that the textural properties of ceramsite coated with micro-Cu_2O catalyst are much better than ceramsite only.

1-4. UV-vis Adsorption

The UV-vis adsorption spectra of samples were measured, and the results shown in Fig. 5. Absorption peaks of the ceramsite coated with micro-Cu_2O catalyst appear around 420 nm and 550 nm. By contrast, the absorption spectrum of ceramsite was slightly changed throughout the whole investigation. The wavelength confirmed that ceramsite was insensitive to illumination variation. Fig. 5 also reflected that the catalyst had much larger absorption range and stronger adsorption intensity in visible-light than ceramsite. This may be attributed to the fact that when micro-Cu_2O was coated on ceramsite, it improved the adsorption capacity of visible-light. Furthermore, the surface morphology of ceramsite and crystalline phases of micro-Cu_2O would be greatly affecting UV-vis absorption [41]. Thus, the test results show that the ceramsite coated with micro-Cu_2O catalyst has high utilization efficiency of visible-light, and is consistent with the previously published results [42], indicating that it may be a preferable photocatalytic material for wastewater treatment.

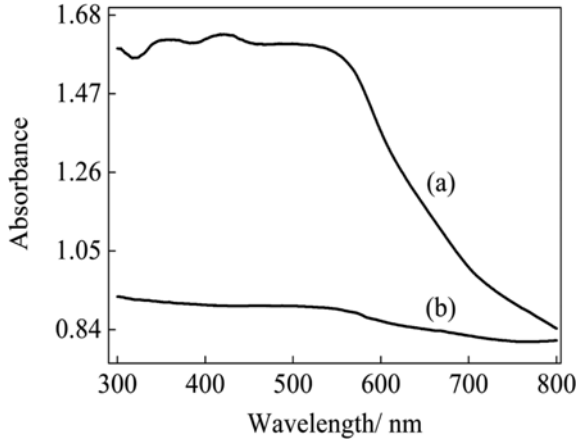

Fig. 5. UV-vis adsorption spectra of (a) ceramsite coated with micro-Cu_2O catalyst and (b) ceramsite.

2. Photocatalytic Activity

2-1. Effect of Initial pH

The variation of initial pH should be considered in the treatment of dye wastewater by means of photo-catalyzed oxidation, for the following reasons. One is that dye wastewater which is discharged from industries has a wide range of pH values. The other is that the generation of hydroxyl radicals is affected by pH conditions [43]. So, the effect of initial pH was investigated on the efficiency of the degradation process in the pH range of 3-11, and the results collected in Fig. 6(a). After 20 min adsorption equilibrium, the removal rates of MB under acidic (pH=3), neutral (pH=7) and alkaline conditions (pH=11) were 61.65%, 28.24% and 50.32%, respectively, suggesting that under acidic or alkaline conditions, the ceramsite coated with micro-Cu_2O catalyst had a good adsorption efficiency for MB. However, under neutral condition, the adsorption efficiency of the catalyst for MB decreased dramatically. Fig. 6(a) also shows that when initial pH was 3, 7 and 11, the deg-

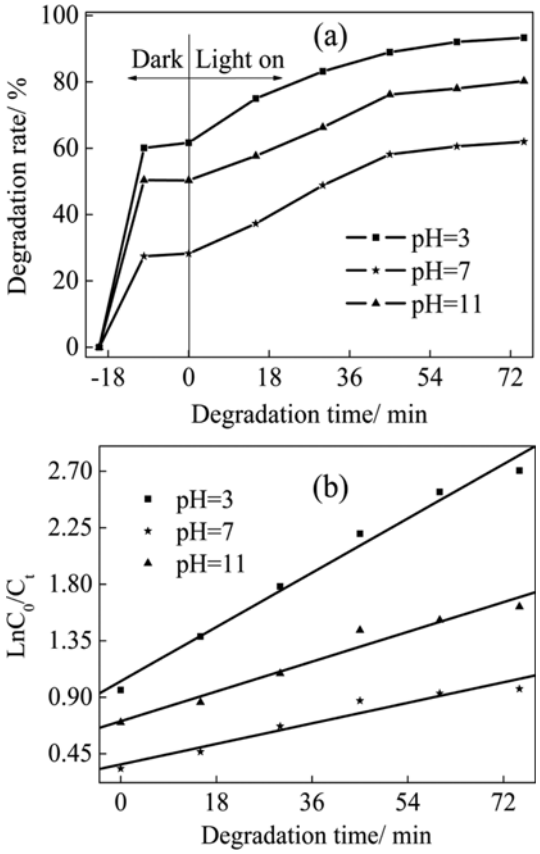

Fig. 6. (a) Effect of initial pH on the degradation of MB by ceramsite coated with micro-Cu_2O catalyst and (b) pseudo-first-order plot for the photocatalytic degradation of MB by the catalyst under Xe light with different initial pH (experimental conditions: initial concentration of MB was 15 mg/L and stirring time was 95 min).

radation rates of MB increased rapidly along with irradiation time and reached about 93.13%, 61.99% and 80.25%, respectively, after Xe light illuminated for 75 min.

We discovered that the adsorption process was essential before the photocatalytic degradation process, mainly because the ceramsite coated with micro-Cu_2O catalyst has enrichment impact on MB, due to its high BET specific surface area and developed porous structure. MB is more easily photocatalytically degraded by valence band holes, conduction band electrons or ·OH, when a certain amount of MB was adsorbed onto the surface and pores of the catalyst. Also, the degradation rate of MB under acidic condition was much higher than that of under neutral pH condition; similar results were also obtained by Şahin et al. [44]. This may be because under neutral condition, the photocatalytic activity of micro-Cu_2O was inhibited by means of Cu(I) capture of the conduction band (e^-_{CB}) to form lower valence state Cu(0) or was oxidized by O_2 in the solution to higher valence state Cu(II) [45].

2-2. Effect of Initial Concentration

The effect of initial concentration of MB on the photocatalytic degradation efficiency was studied over the initial concentration range of 5-30 mg/L, and the results listed in Fig. 7(a). The results illustrate that after 20 min adsorption equilibrium, the removal rates for the initial concentrations of 5, 15 and 30 mg/L were 79.67%, 61.65% and 46.16%, respectively. The observed removal rates decreased along with adsorption time at higher initial concentration, probably due to the rapid exhaustion of the sorption sites of adsorbent [46]. During the photocatalytic degradation process, the degradation rate of MB also decreased with increasing the initial concentration. After Xe light irradiated for 75 min, the degradation rate of MB for the initial concentration of 5 mg/L was higher than that of 30 mg/L, about 10%. Because of higher concentration of MB in the solution, the photons would be absorbed by the MB molecules before they could reach the catalyst surface. This in turn reduced absorption of photons by the catalyst and consequently the discoloration efficiency [47].

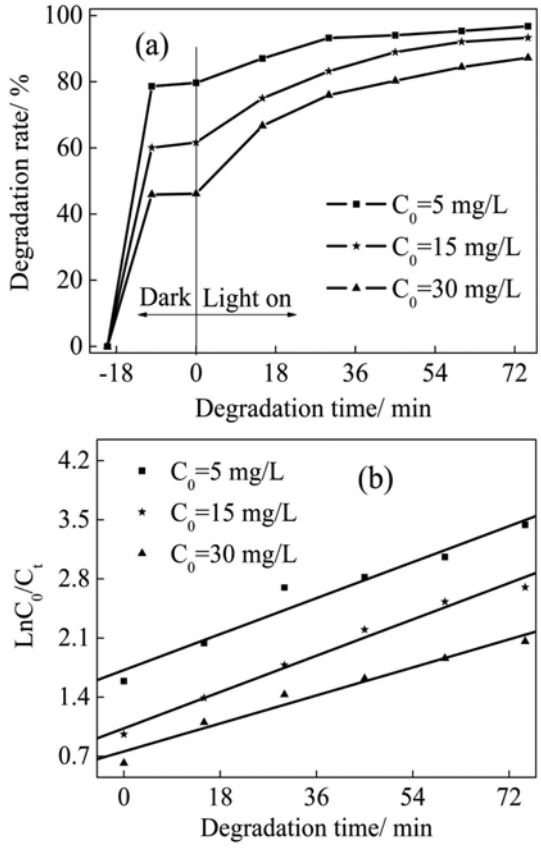

Fig. 7. (a) Effect of initial concentration on the degradation of MB by ceramsite coated with micro-Cu_2O catalyst and (b) pseudo-first-order plot for the photocatalytic degradation of MB by the catalyst under Xe light with different initial concentrations (experimental conditions: initial pH was 3 and stirring time was 95 min).

3. Kinetics Analysis

To further investigate the photocatalytic performance, the degradation kinetics of MB by ceramsite coated with micro-Cu_2O catalyst under Xe light was analyzed. Some studies reported that at low initial concentration of MB, the photocatalytic degradation fitted with the pseudo-first-order kinetics [48,49], evaluated by using the following equation:

$$\ln\left(\frac{C_0}{C_t}\right) = kt \quad (4)$$

where k is the pseudo-first-order rate constant, min^{-1}.

The pseudo-first-order kinetics model of photocatalytic degradation for MB with different initial pH and concentration is presented in Fig. 6(b) and Fig. 7(b), respectively. As Table 2 and Fig. 6(b) detail, under acidic and alkaline conditions, the photocatalytic degradation of MB could be well described by pseudo-first-order kinetics, according to the correlation coefficients (R^2>0.95). However, under neutral condition, the photocatalytic degradation of MB could not be accurately described by the kinetics, because the correlation coefficient is relatively low (R^2<0.95). Furthermore, the effect of initial pH on pseudo-first-order rate constant, 'k', was especially significant. When initial pH was raised from 3 to 7, the k was reduced by 2.64 times, implying that acidic or alkaline condition was propitious to photocatalytic degradation reaction.

As Table 2 and Fig. 7(b) show, the linearity of the plot with regression coefficient, R^2>0.95, indicates that the photocatalytic degradation of MB obeyed the pseudo-first-order kinetics model for all initial concentrations. With the increase of initial concentration, the

Table 2. Pseudo-first-order rate constants (k) for different initial pH and concentrations of MB

Experimental conditions	$k\times10^{-3}$ (min^{-1})	R^2
Initial pH		
3	24	0.985
7	9.1	0.943
11	13.2	0.964
Initial concentrations		
5	23.7	0.956
15	23.9	0.985
30	18.4	0.968

Note: R^2 is the correlation coefficient

change of the k was not obvious. In brief, compared with initial concentration, the effect of initial pH on the photocatalytic activity of the ceramsite coated with micro-Cu_2O catalyst is more remarkable.

4. Degradation Mechanism

A possible photocatalytic degradation mechanism of MB by the ceramsite coated with micro-Cu_2O catalyst was discussed. When micro-Cu_2O was irradiated with a photon of energy greater than its band gap energy, photogenerated electron-hole pairs were formed in the conduction band (e^-_{CB}) and valence band (h^+_{VB}), as shown in Eq. (5) [50]. The photogenerated e^-_{CB} and h^+_{VB} oxidized MB into inorganic or nontoxic materials directly, as listed in Eqs. (6) and (8). With micro-Cu_2O coating on ceramsite, more photo-generated e^-_{CB} could be captured by adsorbed O_2 on the surface of ceramsite to yield H_2O_2 (Eq. (7)), which directly degraded MB (seen Eqs. (10) and (11)). The photo-generated h^+_{VB} react with the OH^- derived from Eq. (8) and form ·OH, seen in Eq. (9). The formation of oxidative intermediate ·OH is very reactive due to its unstable form and acts as a strong oxidizing agent [51], and thus it oxidizes MB into CO_2 and H_2O, as presented in Eq. (10).

$$Cu_2O+hv \rightarrow Cu_2O(e^-_{CB}+h^+_{VB}) \quad (5)$$

$$Cu_2O(e^-_{CB})+MB \rightarrow Products \quad (6)$$

$$Cu_2O(e^-_{CB})+2H_2O+O_2 \rightarrow H_2O_2+2OH^- \quad (7)$$

$$Cu_2O(h^+_{VB})+MB \rightarrow Products \quad (8)$$

$$Cu_2O(h^+_{VB})+OH^- \rightarrow Cu_2O+\cdot OH \quad (9)$$

$$\cdot OH+MB \rightarrow CO_2+H_2O \quad (10)$$

$$H_2O_2+MB \rightarrow Products \quad (11)$$

5. Degradation Pathway

To determine the products, as mentioned in Eqs. (6), (8) and (11), GC-MS and IC apparatuses were used to identify photocatalytic degradation products of MB by ceramsite coated with micro-Cu_2O catalyst under Xe light. As Fig. 8 displays, there were two main characteristic peaks in each investigation. The characteristic peaks at the retention times of 13.41 and 16.33 min after being illuminated for 10 min, the degradation intermediates were made up primarily of 2,4-Di-tert-butylphenol and diisobutyl phthalate, respectively. After being irradiated for 20 min, the degradation intermediates were mainly composed of ε-caprolactone and butyl methacrylate, the characteristic peaks at the retention times of 16.28 and 17.15 min, respectively. Similarly, at the retention times of 13.40 min and 19.75 min irradiating for 40 min, N, N-dimethyl-

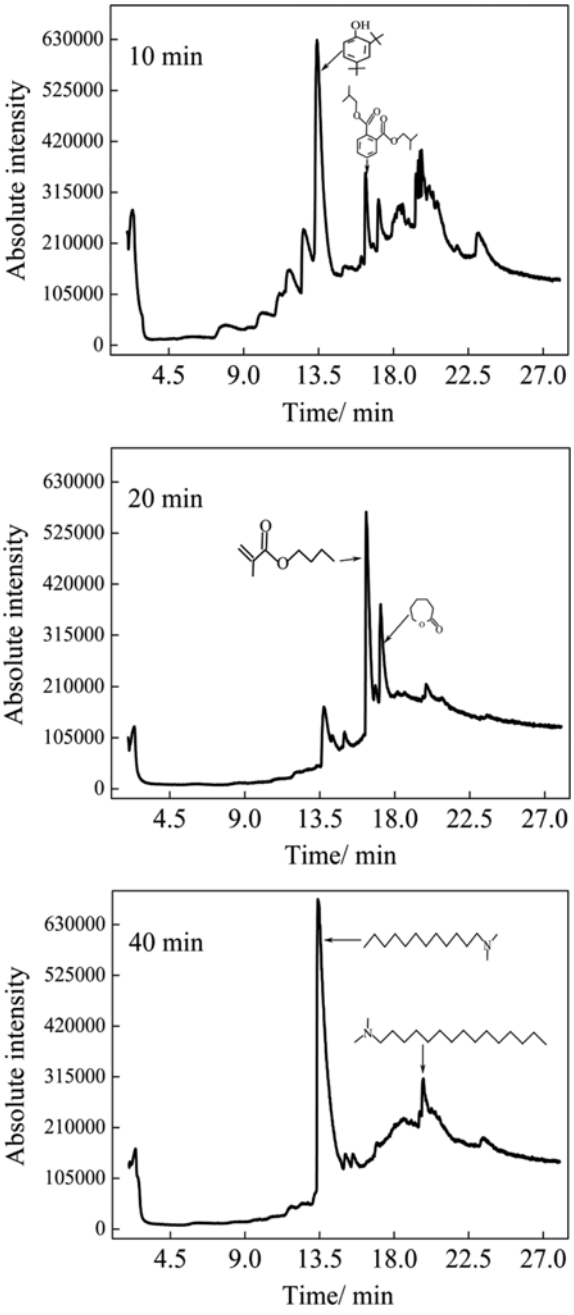

Fig. 8. GC-MS spectra of MB degradation intermediates using ceramsite coated with micro-Cu_2O catalyst under Xe light irradiated for 10, 20 and 40 min (experimental conditions: initial concentration of MB was 15 mg/L and pH was 3).

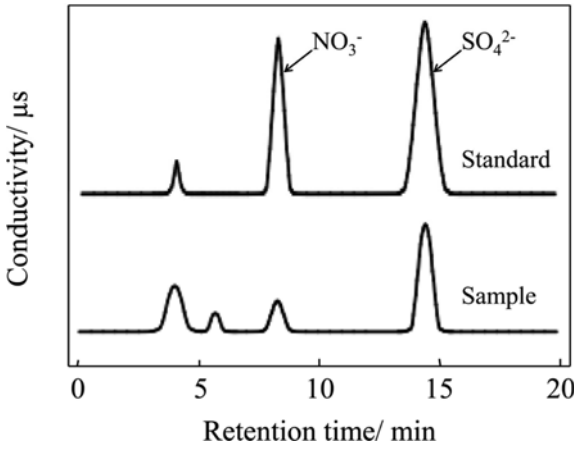

Fig. 9. IC spectra of MB degradation products using ceramsite coated with micro-Cu_2O catalyst under visible-light irradiated for 75 min (experimental conditions: initial pH was 3 and concentration of MB was 15 mg/L).

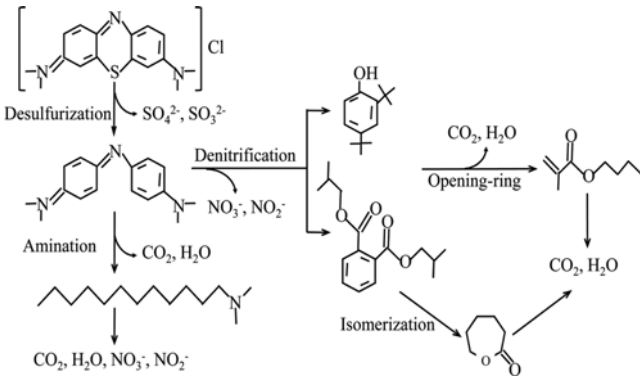

Fig. 10. Degradation pathways of MB by ceramsite coated with micro-Cu_2O catalyst under Xe light.

dodecanamide and N, N-dimethyldodecylamine were the major degradation intermediates, respectively. Besides, we have inferred that with the increase of irradiation time, the species and amount of the degradation intermediates were declining, because the number of peaks were decreasing with the irradiation time increased from 10 min to 40 min, except for characteristic peaks. Based on the analysis of GC-MS, we deduced that in the photocatalytic degradation process, the degradation intermediates of MB were mainly composed of phenols, esters and amines. Moreover, as Fig. 9 indicates, compared with the standard IC spectrum, negative inorganic ions generated in the degradation of MB in the filtrate were SO_4^{2-} and NO_3^-, and may also have been sulfite (SO_3^{2-}) and nitrite (NO_2^-).

Finally, based on the results of Fig. 8 and Fig. 9, the degradation pathways of MB during the photocatalytic degradation process were proposed. As Fig. 10 details, MB was determined to be degraded through two different pathways in the photocatalytic degradation process. The first degradation pathway was that the desulfurization reaction occurred first and then amination reaction took place, and finally MB depredated into CO_2, H_2O, and other inorganic compounds. The other degradation pathway was that after desulfurization reaction, denitrification and opening-ring reactions successively followed, and finally MB was degraded to CO_2 and H_2O. The degradation pathway of MB during the photocatalytic degradation process in the present study was in line with previous researches [52,53].

CONCLUSIONS

A novel ceramsite coated with micro-Cu_2O catalyst, with excellent photocatalytic activity, can be obtained by micro-Cu_2O coating on ceramsite via dipcoating method, and does not require special reagents, expensive equipment or harsh condition. Hence, the coating method can be considered as a facile and green synthesis route.

The high degradation efficiency of the ceramsite coated with micro-Cu_2O catalyst for MB in aqueous solution under visible-light irradiation may be attributed to the synergistic effect of ceramsite and micro-Cu_2O. The former has the advantage of good mass transfer effect, and the latter exhibits strong visible-light adsorption capacity. Besides, GC-MS and IC results clearly demonstrated that phenols, esters and amines were produced as degradation intermediates, and SO_4^{2-} and NO_3^- were generated as the desired products. The degradation pathways of MB were proposed during the photocatalytic degradation process, containing two different ways that occurred simultaneously.

ACKNOWLEDGEMENTS

We thank the Fundamental Research Funds for the Central Universities of China (No. 15D111321) and "Textile Light" Application Basic Research of China (No. J201503).

REFERENCES

1. R. Davide, D. Daniele, F. Maurizio and A. Angelo, *Chem. Soc. Rev.*, **38(7)**, 1999 (2009).
2. T. Cetinkaya, L. Neuwirthová, K. M. Kutláková, V. Tomášek and H. Akbulut, *Appl. Surf. Sci.*, **279**, 384 (2013).
3. Q. Sun, F. Xiao, S. Ren, Z. Dong and X. W. Su, *Ceram. Int.*, **40**, 11447 (2014).
4. C. C. Wang, J. R. Li, X. L. Lv, Y. Q. Zhang and G. S. Guo, *Energy Environ. Sci.*, **7**, 2831 (2014).
5. L. Ren, Z. Jin, W. Wang, H. Liu, J. Lai and J. Yang, *Appl. Surf. Sci.*, **258**, 1353 (2011).
6. A. D. Paola, E. García-López, G. Marcì and L. Palmisano, *J. Hazard. Mater.*, **211**, 3 (2012).
7. Y. Li, B. Wang, S. Liu, X. Duan and Z. Hu, *Appl. Surf. Sci.*, **324**, 736 (2015).
8. X. Shen, S. Chen, D. Mu, B. Wu and F. Wu, *J. Power Sources*, **238**, 173 (2013).
9. A. E. Kasmi, Z. Y. Tian, H. Vieker, A. Beyer and T. Chafik, *Appl. Catal. B-Environ.*, **186**(10), 10 (2016).
10. M. A. Bhosale, T. Sasaki and B. M. Bhanage, *Catal. Sci. Technol.*, **4**(12), 4274 (2014).
11. Y. T. Wang, Y. Q. Pei, W. F. Xiong, T. G. Liu, J. Li and S. L. Liu, *Int. J. Biol. Macromol.*, **81**, 477 (2015).
12. L. Liu, L. Ding, Y. G. Liu, W. J. An, S. L. Lin and Y. H. Liang, *Appl. Surf. Sci.*, **364**, 505 (2016).
13. M. A. Bhosale and B. M. Bhanage, *Adv. Powder Technol.*, **27**, 238 (2016).
14. M. K. Corbierre, N. S. Cameron, M. Sutton, S. G. Mochrie, L. B. Lurio and A. Rühm, *J. Am. Chem. Soc.*, **123**, 10411 (2001).
15. D. M. Zhang, B. S. Hu, D. J. Guan and Z. T. Luo, *Catal. Commun.*, **76**, 7 (2016).
16. S. Gelover, L. A. Gomez and K. Reyes, *Water Res.*, **40**, 3274 (2006).
17. J. F. Ma, J. F. Ding, L. Y. Li, J. Zou, Y. Kong and K. Sridhar, *Ceram. Int.*, **41**, 3191 (2015).
18. K. Laursen, T. J. White, D. J. Cresswell, P. J. Wainwright and J. R. Barton, *J. Environ. Manage.*, **80**(3), 208 (2006).
19. A. M. Mittelman, D. S. Lantagne, J. Rayner and K. D. Pennell, *Environ. Sci. Technol.*, **49**(14), 8515 (2015).
20. S. Maschio, E. Furlani, G. Tonello, N. Faraone, E. Aneggi and D. Minichelli, *Waste Manage.*, **29**(11), 2880 (2009).
21. Y. Z. Zhuang, C. Y. Chen and T. Ji, *Constr. Build. Mater.*, **46**, 13 (2013).
22. E. Furlani, G. Tonello, S. Maschio, E. Aneggi, D. Minichelli and S.

Bruckner, *Ceram. Int.*, **37**, 1293 (2011).
23. C. Wang and F. S. Zhang, *Mater. Lett.*, **93**, 380 (2013).
24. A. Larbot, M. Bertrand, S. Marre and E. Prouzet, *Sep. Purif. Technol.*, **32**, 81 (2003).
25. Y. X. Zhao, Y. N. Yang, S. J. Yang, Q. H. Wang, C. P. Feng and Z. Y. Zhang, *J. Colloid Interface Sci.*, **393**, 264 (2013).
26. C. Jiang, L. Y. Jia, B. Zhang, Y. L. He and K. George, *J. Environ. Sci.*, **26**, 466 (2014).
27. Y. Shi, K. Sun, X. B. Qi and Q. Gao, *J. Wuhan University Technol.-Mater. Sci. Ed.*, **30**(3), 649 (2015).
28. Y. Cheng, W. J. Fan and L. Guo, *Sep. Purif. Technol.*, **130**, 167 (2014).
29. M. Wegmann, B. Michen, T. Luxbacher, J. Fritsch and T. Graule, *Water Res.*, **42**(6), 1726 (2008).
30. Y. Zhang, F. He, S. B. Xia, L. W. Kong, D. Xu and Z. B. Wu, *Ecol. Eng.*, **64**, 186 (2014).
31. S. Qiu, X. Huang, S. W. Xu and F. Ma, *Appl. Biochem. Biotechnol.*, **176**, 267 (2015).
32. T. P. Li, T. T. Sun and D. X. Li, *J. Mater. Cycles Waste Manage.*, DOI:10.1007/s10163-016-0547-3.
33. T. P. Li, T. T. Sun and D. X. Li, *Desalin. Water Treat.*, DOI:10.5004/dwt.2016.0239.
34. Z. Hosseinpour, A. Alemi, A. A. Khandar, X. Zhao and Y. Xie, *New J. Chem.*, **39**(7), 5470 (2015).
35. H. H. Liu, Q. Y. Chen, Y. Yu, Z. H. Liu and G. Xue, *J. Hazard. Mater.*, **263**(2), 593 (2013).
36. W. X. Zou, L. Zhang, L. C. Liu, X. B. Wang, J. F. Sun and S. G. Wu, *Appl. Catal. B-Environ.*, **181**, 495 (2016).
37. D. H. Guo, L. X. Wang, Y. J. Du, Z. Q. Ma and L. Shen, *Mater. Lett.*, **160**, 541 (2015).
38. B. Qin, Y. B. Zhao, H. Li, L. Qiu and Z. Fan, *Chinese J. Catal.*, **36**, 1321 (2015).
39. S. N. Basahel, T. T. Ali, M. Mokhtar and K. Narasimharao, *Nanoscale Res. Lett.*, **10**, 73 (2015).
40. J. S. Valente, F. Tzompantzi, J. Prince, J. G. H. Cortez and R. Gomez, *Appl. Catal. B-Environ.*, **90**, 330 (2009).
41. Y. Y. Xu, X. L. Jiao and D. R. Chen, *J. Phys. Chem. C*, **112**(43), 16769 (2008).
42. C. H. Cao, L. Xiao, C. H. Chen and Q. H. Cao, *Appl. Surf. Sci.*, **357**, 1171 (2015).
43. W. Subramonian and T. Y. Wu, *Water Air Soil Poll.*, **225**(40), 1922 (2014).
44. Ömer Şahin, M. Kaya and C. Saka, *Appl. Clay Sci.*, **116**, 46 (2015).
45. Y. D. Luo, Q. Q. Huang, B. Li, L. H. Dong, M. G. Fan and F. Y. Zhang, *Appl. Surf. Sci.*, **357**, 1072 (2015).
46. O. Ozdemir, M. Turan, A. Z. Turan, A. Faki and A. B. Engin, *J. Hazard. Mater.*, **166**, 647 (2009).
47. D. Zhao, G. Sheng, C. Chen and X. Wang, *Appl. Catal. B-Environ.*, **111**, 303 (2012).
48. F. C. F. Low, T. Y. Wu, C. Y. Teh, J. C. Juan and N. Balasubramaniam, *Color Technol.*, **128**(1), 44 (2012).
49. P. Dumrongrojthanath, A. Phuruangrat, P. Junploy, S. Thongtem and T. Thongtem, *Res. Chem. Intermediat.*, **42**, 1651 (2016).
50. J. K. Dong, H. Y. Xu, F. J. Zhang, C. Chen, L. Liu and G. T. Wu, *Appl. Catal. A-Gen.*, **470**, 294 (2014).
51. D. Gümüş and F. Akbal, *Water Air Soil Poll.*, **216**, 117 (2011).
52. R. S. Dariani, A. Esmaeili, A. Mortezaali and S. Dehghanpour, *Optik*, **127**, 7143 (2016).
53. Q. Wang, S. L. Tian and P. Ning, *Ind. Eng. Chem. Res.*, **53**, 643 (2014).